*International Journal of Microwave and Wireless Technologies*

**cambridge.org/mrf**

# Planar mmWave near-field antenna measurement system with multiple probes

Martin Obermaier[1], Johannes Lange[2], Thomas Deckert[2], Marc Vanden Bossche[3] and Dirk Plettemeier[1]

[1]Chair for RF and Photonics Engineering, Technische Universität Dresden, Dresden, Germany; [2]Emerson/NI, Dresden, Germany and [3]Antennex, Utrecht, Netherlands

**Research Paper**

**Cite this article:** Obermaier M, Lange J, Deckert T, Vanden Bossche M, Plettemeier D (2026) Planar mmWave near-field antenna measurement system with multiple probes. *International Journal of Microwave and Wireless Technologies*, 1–7. https://doi.org/10.1017/S1759078726103808

Received: 12 January 2026 UTC
Revised: 17 July 2026 UTC
Accepted: 31 July 2026 UTC

**Keywords:**
antenna design; microwave measurements; modeling and measurements; NF; RF front-ends

**Corresponding author:** Martin Obermaier; Email: martin.obermaier@tu-dresden.de

**Abstract**

Planar near-field (NF) scanners are an essential tool to measure and characterize antennas. Their compact design and simple operation principle give them an advantage over classical far-field systems. This work presents a compact planar mmWave scanner, which implements an active probe array to achieve better and faster scans. The scanner architecture and the necessary steps to align the NF samples are discussed with a special focus on a novel concept to implement a probe compensation algorithm for multiple probes using a calibration antenna.

## Introduction

Array antennas operating at mmWave frequencies have become widespread in modern communication and remote sensing applications. A major challenge during the production of these antennas is the verification and alignment of every antenna element. Large volume productions require fast and reliable measurement hardware that saves expensive floor space in production environments. Classical far-field (FF) scanners or even compact antenna test ranges are too slow and voluminous for high throughput scenarios. We have previously presented a compact active probe array structure (PAS), which is able to reconstruct the FF behavior of electrically steered antenna arrays (ESAs) based on their near-field (NF) coupling behavior in both RX and TX mode [1, 2]. The algorithm used to reconstruct the FF patterns and behaviors requires knowledge about the single-element radiation patterns of a known reference ESA. This requirement motivated the idea to use the active PAS, which was previously only used to measure the NF coupling, as a multi-probe NF scanning device on a compact planar mmWave NF scanner. Such a scanner would allow us to capture the single-element radiation pattern of the reference ESA without the need for an additional measurement setup to capture the NF coupling. While planar NF scanners allow for very compact measurement setups, the maximum reconstruction angle and overall measurement time are dependent on the dimensions of the scanning plane [3]. Additionally, it is necessary to perform a probe correction on the captured NF data to eliminate the effects of the utilized NF probe during the NF measurement. The steps necessary to achieve probe correction for single-probe NF measurements are very well understood and straight forward to implement as long as the FF pattern of the probe is known [4]. Multi-probe NF systems require more attention, since shading effects and multiple reflections between the individual probes are possible, but multi-probe systems can offer the advantage of faster measurement times and higher signal-to-noise ratios compared to single-probe systems [5].

Another important requirement for our previously presented active PAS algorithms is the correct preservation of the phase information (electric offsets) between the individual single-element antennas of the ESA [1, 2]. Our previous work on FF phase reconstruction from planar NF measurements illustrates and discusses the necessary steps and approaches to preserve this phase information during the NF to FF transformation [6]. In this paper, we describe how a multi-probe NF scanner, based around the previously published active PAS hardware, can be implemented and how the NF needs to be processed in order to reconstruct the correct FF patterns. This work is structured as follows: In "Measurement setup" section, we will explain the measurement setup used to capture the NF and describe the ESA antenna. In "NF processing" section, we will explain and discuss the necessary steps to condition and process the NF captures by the individual NF probes. "Multi-probe correction" section will describe the procedure to perform a probe compensation on the processed NF samples. "Measurement results" section will present the reconstructed FF measurement results of a $4 \times 4$ ESA, shown in Fig. 1, and compare them to a true FF measurement. "Conclusion" section will provide a conclusion. An earlier version of this paper was presented at EuMW 2025 and was published in its Proceedings [7].

© The Author(s), 2026. Published by Cambridge University Press in association with The European Microwave Association. This is an Open Access article, distributed under the terms of the Creative Commons Attribution licence (http://creativecommons.org/licenses/by/4.0), which permits unrestricted re-use, distribution and reproduction, provided the original article is properly cited.

Downloaded from https://www.cambridge.org/core. UNIVERSIDAD AUTONOMA METROPOLITANA, on 19 Nov 2026 at 08:14:32, subject to the Cambridge Core terms of use, available at https://www.cambridge.org/core/terms. https://doi.org/10.1017/S1759078726103808

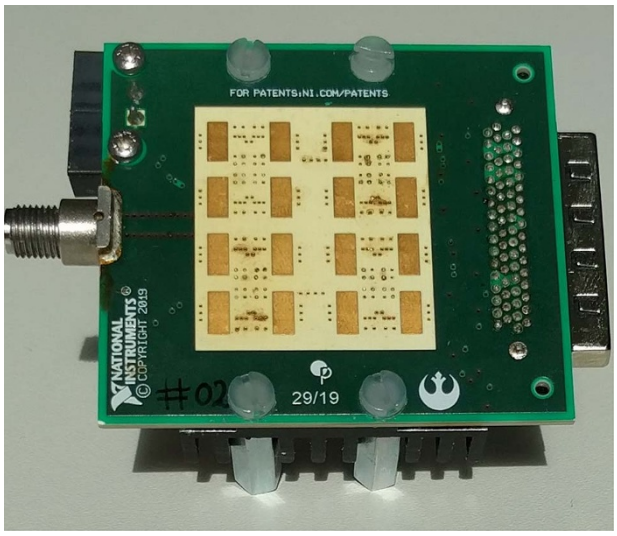



**Figure 1.** $4 \times 4$ ESA antenna operating at 26–30 GHz.

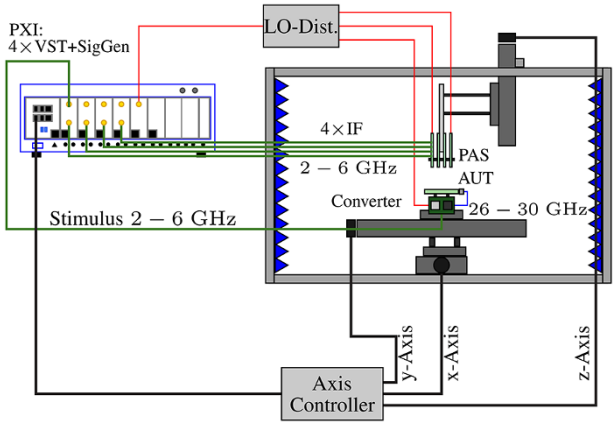



**Figure 2.** Overview of the multi-probe NF scanner.

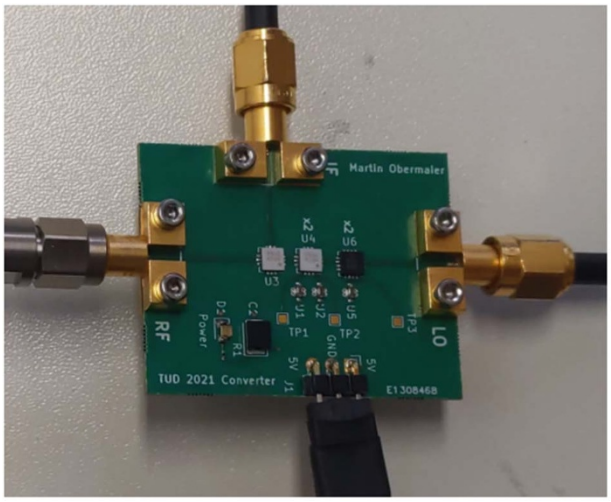



**Figure 3.** Frequency converter PCB operating at 26–30 GHz (RF), 2–6 GHz (IF), and an LO of 6 GHz.

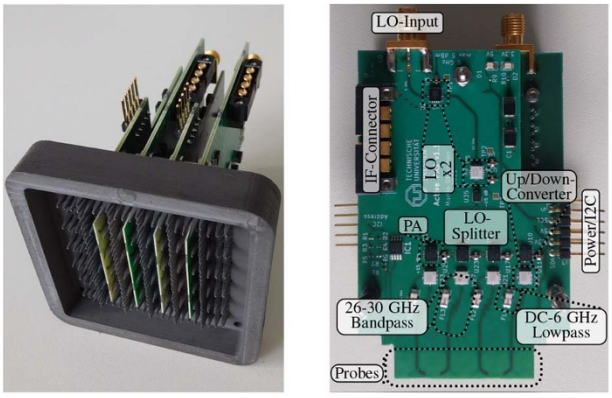



**Figure 4.** Active PAS, with 16 NF probes (4×4 layout).

## Measurement setup

### *Multi-probe NF scanner*

The diagram shown in Fig. 2 illustrates the multi-probe NF scanner setup used in this work. The NF scanner is constructed within a cage of extruded aluminum and uses three linear axes to position the antenna under test (AUT) and the active PAS relative to each other. The $x$- and $y$-axes span a planar scan area of $200 \times 200\,mm$. The $z$-axis has $95\,mm$ of travel and allows to vary the $z$-distance between AUT and active PAS. In contrast to the general construction of planar NF scanners, we have chosen to move the AUT rather than the probe array. This decision was motivated by the number of radio frequency (RF) connections to the active PAS and their routing. This approach is feasible, since in comparison to a spherical or cylindrical scan setup, a planar scan setup only changes the absolute distance between AUT and probe and not the orientation. The movement of probe and AUT are therefore algorithmically interchangeable. The cage and surfaces inside of the scanner are lined with absorber materials to minimize the contributions of reflections to the NF scan. The multi-probe NF scanner measurement system uses a PCI eXtensions for Instrumentation system with four Vector Signal Transceivers (VSTs) to generate a stimulus for the AUT, the local oscillator (LO) for the active PAS and the converter printed circuit board (PCB) as well as capturing data from the probes. The VSTs are able to produce and process modulated signals from 2 to 6 GHz with 1 GHz bandwidth. These intermediate frequencies (IFs) are mixed with the common LO on a converter PCB, shown in Fig. 3, to the desired 26–30 GHz. The active PAS converts the mmWave signals back to the 2–6 GHz band. The converter PCB and active PAS are using identical converter architectures. The lower IF limits the effects of phase drifts and cable losses during the scan, while still enabling broadband measurements with the VSTs.

### *Probe array*

Figure 4 shows the active PAS in detail. The active PAS currently supports up to 16 NF probe channels, which are able to operate between 26 and 30 GHz. The detailed construction and design choices of the active PAS are described and discussed in [1]. Due to the limited number of IF channels on the VST system, we utilize only 4 of the 16 NF probes, and the active PAS provides to capture the NF of the AUT in this work. To maximize the scan area, we have chosen the four outermost corner elements of the probe array. The

Downloaded from https://www.cambridge.org/core. UNIVERSIDAD AUTONOMA METROPOLITANA, on 19 Nov 2026 at 08:14:32, subject to the Cambridge Core terms of use, available at https://www.cambridge.org/core/terms. https://doi.org/10.1017/S1759078726103808

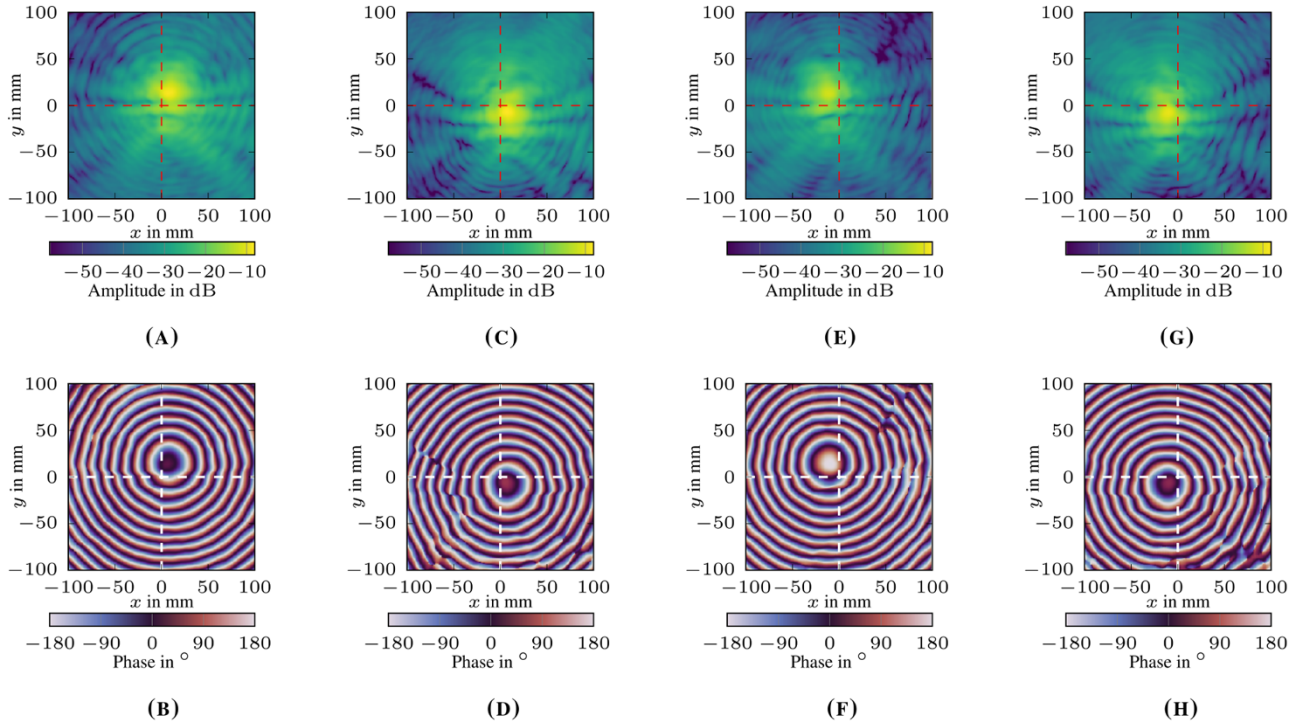



**Figure 5.** NF capture of the main polarization of the reference antenna at 28 GHz. (A) Amplitude probe 1. (B) Phase probe 1. (C) Amplitude probe 2. (D) Phase probe 2. (E) Amplitude probe 3. (F) Phase probe 3. (G) Amplitude probe 4. (H) Phase probe 4.

number of probes could be increased by utilizing an RF switch-matrix without the need of additional IF channels. Additionally, since the PAS is currently only able to measure a single polarization component at a time during a NF scan, we need to rotate the AUT by 90° to capture co- and cross-polarization components of the AUT.

The NF measurement setup shown in this work should only be seen as an exemplary implementation of a planar multi-probe NF scanner. The principles and algorithms presented in this work can be transferred to other planar multi-probe scanners with similar constructions. There is also no need for a frequency conversion step or interchanging the movement of AUT and probes. We chose to reuse the ESA and active PAS in this work out of pragmatisms and our overall goal to expand the capabilities of the active PAS and the stationary NF to FF algorithms presented in [1, 2].

## NF processing

Figure 5 shows the NF amplitude and phase of a reference patch antenna captured by the four corner probes of the active PAS. The reference patch antenna fulfills multiple purposes during the NF processing steps. The main purpose of the reference patch antenna is to spatially align the captured NF samples in the *xy*-plane and correct for electrical offsets in the IF path of the active PAS. Furthermore, the reference patch antenna is also essential to perform the multi-probe compensation. Due to the construction of the active PAS, we cannot ensure the exact relative spatial offsets of each NF probe to the other probes in the array. But these relative spatial offsets can be reconstructed from the individual NF phase captures of each probe, given the knowledge that they are scanning the same AUT at the same $z$ distance. We are able to obtain these relative spatial offsets between the probes by calculating the phase center of the reference antenna in the *xy*-plane for each NF capture [6]. This can be achieved by using a 2D phase unwrap algorithm and calculating a phase centroid for a given iso-phase [8]. The antenna used during these measurements needs be well behaved in its phase pattern (e.g. radially symmetrical and without phase jumps, which are caused by side lobes) to not introduce errors during the unwrapping.

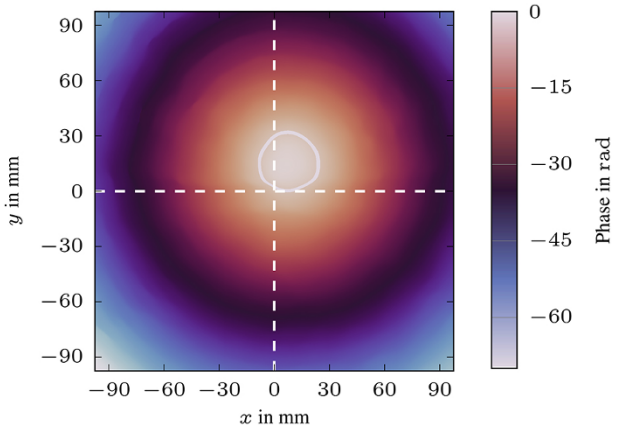



**Figure 6.** Unwrapped phase of NF probe 1 scanning the reference patch antenna.

Figure 6 shows the 2D unwrapped phase of probe 1 along the *xy*-plane, scanning the NF of the reference antenna. The shape highlighted by its white boundary is defined by an iso-phase of $\text{unwrap}(\arg(p1)) = \pi$. It is now possible to determine the relative

Downloaded from https://www.cambridge.org/core. UNIVERSIDAD AUTONOMA METROPOLITANA, on 19 Nov 2026 at 08:14:32, subject to the Cambridge Core terms of use, available at https://www.cambridge.org/core/terms. https://doi.org/10.1017/S1759078726103808

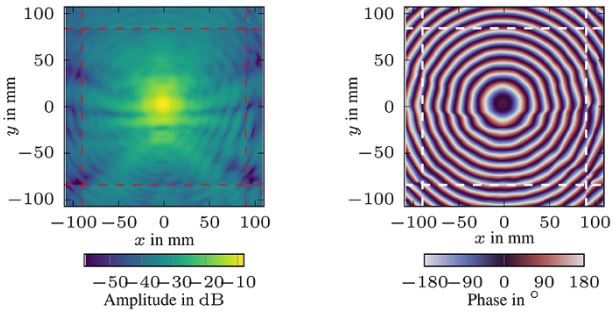



**Figure 7.** Combined NF samples of the reference antenna (primary polarization) at 28 GHz.

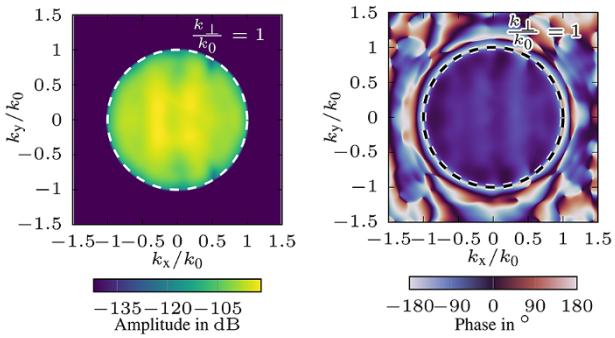



**Figure 8.** Modal spectrum of the reference antenna 28 GHz with no probe correction (main polarization).

offset of each probe and the origin, which is shown by the white cross, by calculating the centroid of this shape using every sample point $(x_i, y_i)$ inside the shape [9].

$$x_0 = \frac{1}{N}\sum_{i=0}^{N-1} x_i \tag{1}$$

$$y_0 = \frac{1}{N}\sum_{i=0}^{N-1} y_i \tag{2}$$

To increase accuracy, the calculation can be repeated for multiple iso-phase values, e.g. $1.5\pi$, $2\pi$, and $3\pi$, and the result can be averaged. Based on the position of the phase centers $(x_{0,i}, y_{0,i})$ in each NF capture, we are able to calculate a complex IF correction factor for each RF channel of the active PAS, which includes the probe and corresponding conversion channel. This complex correction factor is necessary, since each channel of the active PAS has a different electric length and, therefore, introduces a phase and amplitude offset. We denote these corrected NF captures as:

$$\begin{aligned} w_{1,cor}(x,y,z=z_0) &= w_1 \\ w_{2,cor}(x,y,z=z_0) &= w_2 \cdot \frac{w_2(x_{0,2},y_{0,2})}{w_1(x_{0,1},y_{0,1})} \\ w_{3,cor}(x,y,z=z_0) &= w_3 \cdot \frac{w_3(x_{0,3},y_{0,3})}{w_1(x_{0,1},y_{0,1})} \\ w_{4,cor}(x,y,z=z_0) &= w_4 \cdot \frac{w_4(x_{0,4},y_{0,4})}{w_1(x_{0,1},y_{0,1})} \end{aligned} \tag{3}$$

The raw samples $w_i(x, y, z = z_0)$ of main polarization are sampled at a distance $z_0$ and the coordinate $(x_{0,i}, y_{0,i})$ is the location of the phase center in each capture. In an actual implementation of this approach, we would average the samples around this point to calculate the correction factor. The correction factors for the second polarization are identical, since we only rotate the AUT for this measurement and the IF and conversion path is not changed. Based on the calculated offset location $(x_0, y_0)$ of the phase center in each NF capture, it is now possible to superpose the four corrected NF captures. The superposed NF is shown in Fig. 7. In areas where the NF captures of the different probes overlap, the samples are averaged.

The combined NF can now be processed and transformed into the modal space as described in [6]. This also includes an alignment of the combined NF phase center with the origin and windowing of the combined NF. The processed and transformed NF can then be expressed using planar modes as:

$$\begin{aligned} E_x(x,y,z_0) &= \iint_{k_x,k_y} f_x(k_x,k_y) e^{-j(k_x x + k_y y + k_z z_0)} \mathrm{d}k_x \mathrm{d}k_y \\ E_y(x,y,z_0) &= \iint_{k_x,k_y} f_y(k_x,k_y) e^{-j(k_x x + k_y y + k_z z_0)} \mathrm{d}k_x \mathrm{d}k_y \end{aligned} \tag{4}$$

The $z$-component of the wave vector is defined as $k_z = \sqrt{k_0^2 - k_x^2 - k_y^2}$ and $k_0$ is the wavenumber in vacuum. $E_{x,y}$ are the combined and processed NF samples shown in Fig. 7. Figure 8 shows the modal spectrum of the combined and processed NF. The modal spectrum has been corrected for the measurement distance $z_0$ by holographic correction [6].

## Multi-probe correction

To reconstruct the correct FF from the measured modal spectrum shown in Fig. 8, it is necessary to correct the modal spectrum for the influence of the probes used to sample the NF. Every real probe shows directivity, which attenuates some of the measured AUT modes and may also change their phase. To incorporate the effect of probe directivity, Equation 4 has to be rewritten as:

$$\mathbf{E}(x,y,z) = \iint_{k_x,k_y} \mathbf{f}_P(\mathbf{k}) \cdot \mathbf{f}_{AUT}(\mathbf{k}) e^{-j(\mathbf{kr})} \mathrm{d}k_{x,y} \tag{5}$$

$$\mathbf{f}_P(k_x,k_y) = \begin{bmatrix} f_{pp1}(k_x,k_y) & f_{cp1}(k_x,k_y) \\ f_{cp2}(k_x,k_y) & f_{pp2}(k_x,k_y) \end{bmatrix} \tag{6}$$

The modal spectra $f_{pp1,2}$ and $f_{cp1,2}$ are the principle and cross-polarization responses of the probe in the modal spectrum. Since we assume that the same probes measure both principle and cross-polarization responses, we know that $f_{pp1}(\phi) = f_{pp2}(\phi + 90^\circ)$ and $f_{cp1}(\phi) = f_{cp2}(\phi + 90^\circ)$ [10]. The modal spectrum $\mathbf{f}_{AUT}(\mathbf{k})$ describes the true modal spectrum of the AUT. In the case of a single probe, $\mathbf{f}_P(k_x, k_y)$ can be easily calculated from the probe pattern or derived analytically for special probes [11]. This approach is not feasible for a multi-probe NF scanner, since coupling and shading effects cannot be neglected inside the probe array, due to the close proximity of the probes. We are also not able to measure the probe response a classical FF setup due to the construction of the probe array. Instead

Downloaded from https://www.cambridge.org/core. UNIVERSIDAD AUTONOMA METROPOLITANA, on 19 Nov 2026 at 08:14:32, subject to the Cambridge Core terms of use, available at https://www.cambridge.org/core/terms. https://doi.org/10.1017/S1759078726103808

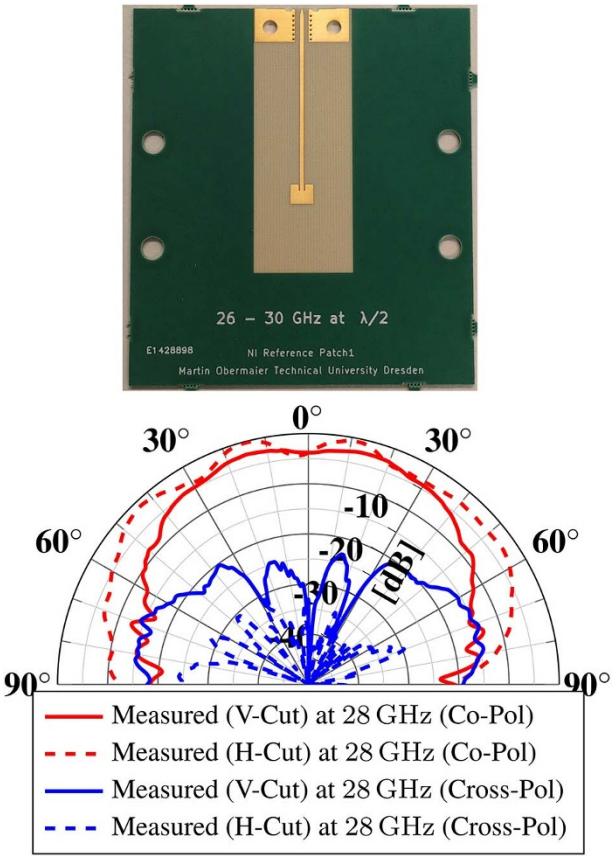



**Figure 9.** Reference antenna pattern designed for 26–30 GHz.

of determining the probe response of every probe in the array, we will characterize the overall response of the complete probe array using a known reference antenna. Since we have measured the true FF of the reference antenna shown in Fig. 9, we are able to calculate the equivalent modal spectrum of the reference antenna. This, in turn, allows us to compute the multi-probe response, which has been defined in Equation 6, from the FF and NF measurements of the reference antenna similar to the approach presented in [10]. The stationary phase approximation allows the approximation of the FF based on the modal spectrum [12]:

$$\begin{aligned} E_\theta(r,\theta,\phi) &\simeq j\frac{k\cdot e^{-jkr}}{2\pi r}\left(f_x\cos(\phi)+f_y\sin(\phi)\right)\\ E_\phi(r,\theta,\phi) &\simeq j\frac{k\cdot e^{-jkr}}{2\pi r}\cos(\theta)\left(-f_x\cos(\phi)+f_y\sin(\phi)\right)\end{aligned} \tag{7}$$

Based on Equation 7, we are able to calculate the modal spectrum of the reference antenna by:

$$\begin{aligned} f_x &= \frac{E_\theta\cos(\phi)-E_\phi\sin(\phi)}{\cos(\theta)}\\ f_y &= \frac{E_\theta\sin(\phi)+E_\phi\cos(\phi)}{\cos(\theta)}\end{aligned} \tag{8}$$

Since there exists a singularity at $\theta = \pm 90°$, it is necessary to limit the spectrum to a value $|\theta| < 90°$. A sensible choice for this limit of $\theta$ is the truncation angle $\theta_v$, which is inherent to planar NF scanners and dependent on the dimensions of the scanning plane and scanning distance between AUT and probe [3].

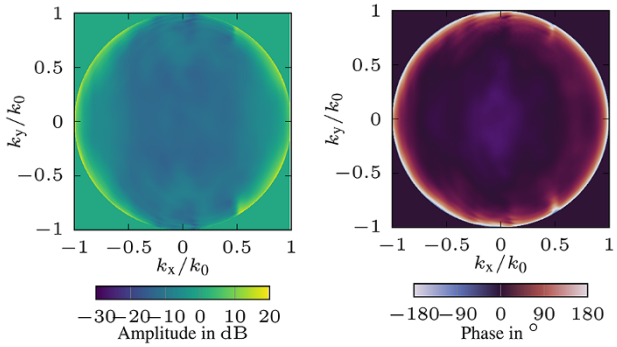



**Figure 10.** Modal correction spectrum at 28 GHz.

Given the measured NF $\mathbf{f}_M(k_x,k_y)$ composed of all probes as well as the true spectrum $\mathbf{f}_{AUT}(k_x,k_y)$ derived from the FF measurement, we are able to calculate the probe response $\mathbf{f}_p(k_x,k_y)$. Using Equations 5 and 6, we can express the relation between $\mathbf{f}_M(k_x,k_y)$ and $\mathbf{f}_{AUT}(k_x,k_y)$ as:

$$\begin{aligned} f_{M,x}(k_x,k_y) &= f_{pp1}(k_x,k_y)\cdot f_{AUT,x}(k_x,k_y)\\ &\quad + f_{cp1}(k_x,k_y)\cdot f_{AUT,y}(k_x,k_y)\\ f_{M,y}(k_x,k_y) &= f_{cp2}(k_x,k_y)\cdot f_{AUT,x}(k_x,k_y)\\ &\quad + f_{pp2}(k_x,k_y)\cdot f_{AUT,y}(k_x,k_y)\end{aligned} \tag{9}$$

Equation 9 is underdetermined with four unknowns and two equations, but since $f_{pp1}(\phi) = f_{pp2}(\phi+90°)$ and $f_{cp1}(\phi) = f_{cp2}(\phi+90°)$ it follows that:

$$\begin{aligned} f_{pp,2}(k_x,k_y) &= f_{pp,1}(-k_y,k_x)\\ f_{cp,2}(k_x,k_y) &= f_{cp,1}(-k_y,k_x)\end{aligned} \tag{10}$$

This allows us to substitute the second equation of Equation 9 by calculating the point $(k_y,-kx)$ and using the properties described in Equation 10. This results in two equations for two unknowns, which allow us to solve for all $f_{pp,1}(k_x,k_y)$ and $f_{cp,1}(k_x,k_y)$. And $f_{pp,2}(k_x,k_y)$ as well as $f_{cp,2}(k_x,k_y)$ can be found by applying Equation 10.

$$\begin{aligned} f_{M,x}(k_x,k_y) &= f_{pp1}(k_x,k_y)\cdot f_{AUT,x}(k_x,k_y)\\ &\quad + f_{cp1}(k_x,k_y)\cdot f_{AUT,y}(k_x,k_y)\\ f_{M,y}(k_y,-k_x) &= f_{cp2}(k_y,-k_x)\cdot f_{AUT,x}(k_y,-k_x)\\ &\quad + f_{pp2}(k_y,-k_x)\cdot f_{AUT,y}(k_y,-k_x)\\ f_{M,y}(k_y,-k_x) &= f_{cp1}(k_x,k_y)\cdot f_{AUT,x}(k_y,-k_x)\\ &\quad + f_{pp1}(k_x,k_y)\cdot f_{AUT,y}(k_y,-k_x)\end{aligned} \tag{11}$$

The overall probe effect for the principle polarization $f_{pp1}(k_x,k_y)$ at 28 GHz is shown in Fig. 10 and can now be applied to the captured NF of any scanned AUT.

## Measurement results

To validate our approach, we measured a $4\times4$ ESA antenna, which is shown in Fig. 1 and operates between 26 and 30 GHz, with the multi-probe NF scanning system as well as with a conventional

Downloaded from https://www.cambridge.org/core. UNIVERSIDAD AUTONOMA METROPOLITANA, on 19 Nov 2026 at 08:14:32, subject to the Cambridge Core terms of use, available at https://www.cambridge.org/core/terms. https://doi.org/10.1017/S1759078726103808

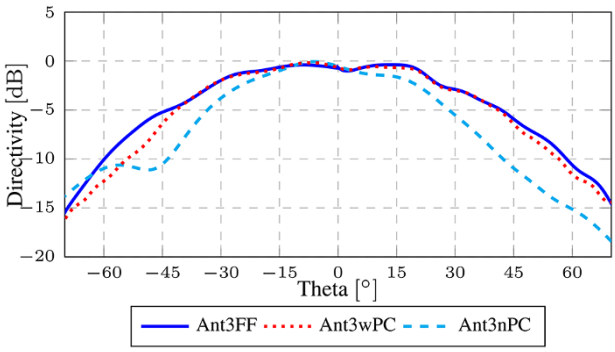



**Figure 11.** Comparison of measured FF, reconstructed FF with and without probe correction of antenna element 3 at 28 GHz (H-Cut).

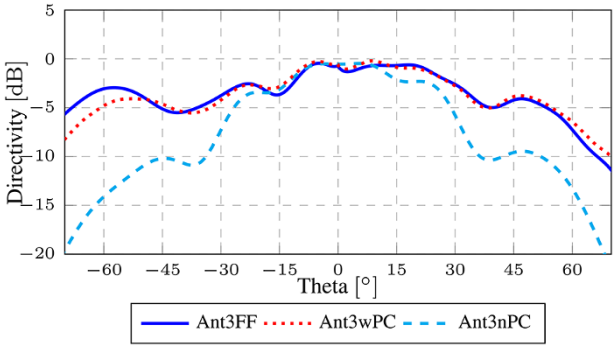



**Figure 12.** Comparison of measured FF, reconstructed FF with and without probe correction of antenna element 3 at 28 GHz (V-Cut).

spherical FF scanner. The ESA is identical to the one used in [1, 2] and [6]. During the measurement only a single element of the ESA was active at a time. Figures 11 and 12 show the FF pattern cut, measured by a spherical scanner (FF), as well as the reconstructed FF from the multi-probe NF scanner with and without probe correction applied to the captured NF for antenna element 3 of the ESA. The figure shows that the reconstructed FF pattern agrees very well with the measured FF pattern up to the angle of validity, which was $\theta_v = 70^\circ$ for this measurement setup. In principle, the scanner could measure a fully active array, but the limited *xy*-travel would limit the angle of validity to below $\theta_v = 38^\circ$ at the necessary measurement distance outside the reactive NF of the fully active ESA.

## Conclusion

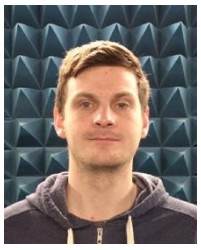
This work shows how a planar multi-probe scanner can be constructed and how the NF samples of the different probes can be spatially and electrically aligned. Additionally, we have presented a novel probe compensation algorithm for multi-probe scanners, which can be implemented and performed with the help of a known reference antenna. This work complements and expands the capabilities of the active PAS, since it is now possible to capture the necessary single-element patterns of the AUT for the NF to FF algorithms presented in [1] and [2] without an additional FF antenna measurement system. Additionally, the system now enables additional diagnostic approaches like holography, which support the applications of the active PAS in research and development applications.

**Acknowledgements.** We would like to acknowledge the contributions of Emerson/NI in the construction and evaluation of multi-probe NF scanner. We are very grateful for the provisioning of the ESAs, VSTs, and the corresponding control system.

**Competing interests.** The authors report no conflict of interest.

## References

1. **Obermaier M, M Laabs, T Deckert and D Plettemeier** (2023) Active probe array structure for assessment of mmWave antenna arrays. In *2023 53rd European Microwave Conference (EuMC)*, Berlin, pp. 190–193.
2. **Obermaier M, J Lange, T Deckert, MV Bossche and D Plettemeier** (2024) Rx characterization of mmwave antenna arrays using an active probe array structure. In *2024 54th European Microwave Conference (EuMC)*, Paris, pp. 704–707.
3. **Newell A** (1988) Error analysis techniques for planar near-field measurements. *IEEE Trans. Antennas Propagat.* **36**(6), 754–768.
4. **Parini C, Gregson S and McCormick J** (2021) *Theory and Practice of Modern Antenna Range Measurements, 2nd Expanded Edition: Volume 1*, IET.
5. **Saccardi F, N Gross, P Iversen, K Hassett, J Hartzell, T Schellenberg, G Pinchuk, R Braun, L Shmidov, S Solomon *et al.*** (2021) Fast multi-probe planar near field measurements with full probe compensation. In *2021 15th European Conference on Antennas and Propagation (EuCAP)*, IEEE, DÜsseldorf, pp. 1–5.
6. **Obermaier M, T Deckert, MV Bossche and D Plettemeier** (2024) Far field phase reconstruction using planar near field scanning techniques. In *2024 15th German Microwave Conference (GeMiC)*, Duisburg, pp. 109–112.
7. **Obermaier M, J Lange, T Deckert, MV Bossche and D Plettemeier** (2025) Compact multi-probe planar near field antenna measurement system. In *2025 55th European Microwave Conference (EuMC)*, Utrecht, pp. 1292–1295.
8. **Herráez MA, Burton DR, Lalor MJ and Gdeisat MA** (2002) Fast two-dimensional phase-unwrapping algorithm based on sorting by reliability following a noncontinuous path. *Applied Optics* **41**(35), 7437–7444.
9. **Protter MH and Morrey CB** (1970) College calculus with analytic geometry.
10. **Masters GF** (1991) Probe-correction coefficients derived from near-field measurements. *AMTA Conference, October* **7**(11).
11. **Gregson S, McCormick J and Parini C** (2007) *Principles of Planar Near-Field Antenna Measurements*. Vol. 53. IET.
12. **Balanis CA** (2015) *Antenna Theory: Analysis and Design*. John Wiley & Sons.



**M. Obermaier** received his M.Sc. in Electrical Engineering from the Karlsruhe Institute of Technology in 2019. He currently works at the chair for RF and Photonics Engineering of the Technical University of Dresden. His main research interests are antenna and microwave measurement techniques.



**J. Lange** is a Principal Engineer at Emerson/NI, where his current research focuses on applying artificial intelligence to wireless communication systems. His previous work includes investigations into over-the-air measurement methodologies and wideband vector network analysis. He has contributed to the development and commercialization of RF test solutions for integrated circuits, wireless devices, and base station technologies. Johannes holds an M.Sc. in Electrical Engineering from Dresden University of Technology (2006).

Downloaded from https://www.cambridge.org/core. UNIVERSIDAD AUTONOMA METROPOLITANA, on 19 Nov 2026 at 08:14:32, subject to the Cambridge Core terms of use, available at https://www.cambridge.org/core/terms. https://doi.org/10.1017/S1759078726103808



**T. Deckert** is a Chief Engineer with Emerson/NI, where he is currently leading research in over-the-air measurement methodology. Prior to that, he held various positions in development and product marketing for solutions to testing RF integrated circuits, wireless devices, and base stations. Thomas holds a Ph.D. degree in Wireless Communications, received from Technische Universität Dresden in 2007, and a M.Sc. degree in Electrical Engineering, received from the University of Wisconsin – Madison in 2002. He is author and co-author of eight patents.



**M. Vanden Bossche** has built up extensive expertise and practical experience in high-frequency large-signal network analysis. He received in 1990 a Ph.D. from Vrije Universiteit Brussel (VUB) in electrical engineering focusing on the foundation of high frequency large-signal network analysis. Also in 1990, he established a Hewlett Packard R&D team at the VUB to further research and develop the technology resulting in 2002 into the spinoff "NMDG." After acquisition by National Instruments (NI) in 2012, Marc has been driving vector calibration techniques and wideband modulation measurements for semiconductor production testers at NI. He became expert and technical lead for forth looking projects related to realistic wideband and over the air characterization (OTA). In January 2025, he brought his expertise to Antennex to make OTA characterization fast, accurate, and still simple for conductive engineers. Marc is a senior IEEE member and ex-chair of IEEE TC3. He was a corecipient of the 2002 ARFTG Technology Award and recipient of two ARFTG Best Paper Awards and is author of 11 patents.



**D. Plettemeier** (Member, IEEE) received the Ph.D. degree in electrical engineering from Ruhr-Universität Bochum, Bochum, Germany. Since 2011, he has been a Full Professor with the Chair of Radio Frequency and Photonics Engineering, Technische Universität Dresden, Dresden, Germany. He has been involved in several international scientific activities, as a Co-Investigator for ESA and NASA Space Missions, such as Cassini-Huygens, Rosetta, and ExoMars, mainly focusing on subsurface imaging. He is currently with the Centre for Tactile, Human-in-the-Loop, and 6G-Life Research Hub, where he is involved in electronics for next-generation sensor and communications systems. His research interests include millimeter-wave and terahertz systems, antennas and chip-integrated applications, microwave photonics, wave propagation, remote sensing, and imaging solutions for radar applications.

Downloaded from https://www.cambridge.org/core. UNIVERSIDAD AUTONOMA METROPOLITANA, on 19 Nov 2026 at 08:14:32, subject to the Cambridge Core terms of use, available at https://www.cambridge.org/core/terms. https://doi.org/10.1017/S1759078726103808